How to cite: *Angew. Chem. Int. Ed.* **2024**, *63*, e202400261
doi.org/10.1002/anie.202400261

Supramolecular Chemistry

Selective Formation of Pd-DNA Hybrids Using Tailored Palladium-Mediated Base Pairs: Towards Heteroleptic Pd-DNA Systems

*Antonio Pérez-Romero, Mario Cano-Muñoz, Carmen López-Chamorro, Francisco Conejero-Lara, Oscar Palacios, José A. Dobado, and Miguel A. Galindo**

Dedicated to Professor Andrew Houlton

Abstract: The formation of highly organized metal-DNA structures has significant implications in bioinorganic chemistry, molecular biology and material science due to their unique properties and potential applications. In this study, we report on the conversion of single-stranded polydeoxycytidine (dC_{15}) into a Pd-DNA supramolecular structure using the [Pd(Aqa)] complex (Aqa = 8-amino-4-hydroxyquinoline-2-carboxylic acid) through a self-assembly process. The resulting Pd-DNA assembly closely resembles a natural double helix, with continuous [Pd(Aqa)(C)] (C = cytosine) units serving as palladium-mediated base pairs, forming interbase hydrogen bonds and intrastrand stacking interactions. Notably, the design of the [Pd(Aqa)] complex favours the interaction with cytosine, distinguishing it from our previously reported [Pd(Cheld)] complex (Cheld = chelidamic acid). This finding opens possibilities for creating heteroleptic Pd-DNA hybrids where different complexes specifically bind to nucleobases. We confirmed the Pd-DNA supramolecular structural assembly and selective binding of the complexes using NMR spectroscopy, circular dichroism, mass spectrometry, isothermal titration calorimetry, and DFT calculations.

Introduction

The integration of DNA into the fabrication of supramolecular assemblies has led to a groundbreaking era in the advancement of nanomaterials.[1–4] Notably, significant attention is focused on advancing metal-DNA systems, wherein the metal entities are precisely arranged along specific sequences. This precision aims to construct dynamic metal-DNA hybrids, gathering significant thought for their potential to stimulate diverse applications.[5–9] In this context, the possibility of scheduling specific sequences for rational self-assembly through base pairs recognition has made DNA an ideal candidate for building highly organized functional systems at the nanoscale. Complementary DNA strands (ds-DNA) are frequently employed for this task, but single-stranded DNA (ss-DNA) can also serve as a template to yield customized supramolecular systems.[10,11] In this scenario, the binding of molecules to ss-DNA has traditionally relied on intermolecular forces acting on the nucleobases or phosphate groups, thus facilitating the assembly of structures. In recent years, this field of research has witnessed remarkable advancements, resulting in noteworthy outcomes.[12] However, the arrangement of metal entities along ss-DNA has received comparatively less attention. Building upon prior knowledge, our research has explored a novel strategy for designing metal-DNA templated systems. We employed specifically designed Pd^{II}-coordination compounds endowed with a unique capability to bind nucleobases along ss-DNA through both coordinating bonds and Watson–Crick complementary hydrogen bonds.[13] While some previous studies focused on the interaction of Pd^{II}-coordination compounds with nucleobases at monomeric level[14–16] or at single-nucleotide gap in double helixes,[17] our strategy aims to precisely organize a continuous one-dimen-

[*] A. Pérez-Romero, C. López-Chamorro, Dr. M. A. Galindo
Departamento de Química Inorgánica. Unidad de Excelencia Química Aplicada a Biomedicina y Medioambiente. Facultad de Ciencias. Universidad de Granada
Avda Fuentenueva s/n, 18071 Granada (Spain)
E-mail: magalindo@ugr.es

Dr. M. Cano-Muñoz, Prof. Dr. F. Conejero-Lara
Departamento de Química Física, Instituto de Biotecnología y Unidad de Excelencia Química Aplicada a Biomedicina y Medioambiente. Facultad de Ciencias. Universidad de Granada
Avda Fuentenueva s/n, 18071 Granada (Spain)

Dr. O. Palacios
Departament de Química, Facultat de Ciències. Universitat Autònoma de Barcelona.
Campus Ballaterra s/n, 08193 Cerdanyola del Vallès, Barcelona (Spain)

Prof. Dr. J. A. Dobado
Grupo de Modelización y Diseño Molecular, Departamento de Química Orgánica. Facultad de Ciencias. Universidad de Granada.
Avda Fuentenueva s/n, 18071 Granada (Spain)

sional array of Pd^{II} ions and ligands along specific ss-DNA sequences. It is noteworthy that these ligands can be customized to create Pd^{II} complexes with tailored substituents, thereby enhancing their affinity for nucleobases and/or introducing enhanced functionalities. The inherent moderate strength of Pd^{II} coordination bonds ensures system stability while allowing for self-correction interactions, guiding the system towards a thermodynamically stable configuration.

We have previously shown that metal complex [Pd(Cheld)(CH_3CN)] (**Pd-Cheld**) (Cheld = chelidamic acid) self-assembles with a single-stranded polydeoxyadenosine (dA_{15}), resulting in the formation of a supramolecular Pd-DNA hybrid structure.[13] Our current research focuses on expanding this strategy to design and synthesize new metal complexes capable of recognizing other nucleobases in DNA sequences. Specifically, we are exploring competitive designs of metal complexes to selectively bind to specific bases, thereby paving the way for developing heteroleptic metal-DNA hybrids.

In this work, we report the synthesis and characterization of complex [Pd(Aqa)(DMSO)] (**Pd-Aqa**) (Aqa = 8-amino-4-hydroxyquinoline-2-carboxylic acid) and demonstrate its capability to bind to cytosine resulting in the formation of Pd-mediated base pair [Pd(Aqa)(Cyt)] (**Cyt-Pd-Aqa**) (Cyt = 1-methylcytosine). Furthermore, we demonstrate that these palladium-mediated base pairs can be prepared on a single-stranded 15mer deoxycytidine (**dC_{15}**) to yield a Pd-DNA helical supramolecular structure. This system comprises continuous **Cyt-Pd-Aqa** base pairs organized similarly to canonical base pairs in DNA double helix. Notably, the Pd^{II} ions are successfully accommodated throughout the double-stranded structure, forming a continuous one-dimensional (1D) metal array (Scheme 1). In addition, we performed competitive binding assays using circular dichroism (CD) titration experiments and isothermal titration calorimetry (ITC) measurements to demonstrate the preferential binding of **Pd-Aqa** to cytosine compared to **Pd-Cheld**. This strategy, using metal complexes complementary to bases, offers exciting possibilities for developing advanced metal-DNA supramolecular hybrids that can be personalized by selecting specific DNA sequences and complementary metal complexes, allowing for rational customization of their structure and properties.

Results and Discussion

The complex **Pd-Aqa** was synthesized in solution by reacting equimolar amounts of $Pd(NO_3)_2$ and the **Aqa** ligand. The formation of the complex was confirmed by ^1H NMR spectroscopy and ESI-MS spectrometry. The changes in the NMR (DMSO-D_6) spectrum provided a means to follow the formation of the complex (Supp. Info., Figure S1–S2). In the presence of increased amounts of Pd^{II} ions, the **Aqa** spectrum shifted downfield, indicating the interaction of the metal ions with the ligand. Upon adding one equivalent of Pd^{II} only signals for a distinct species were observed, with no signals for the free **Aqa** ligand, in agreement with the complete formation of **Pd-Aqa** complex. The solution was subjected to analysis using ESI-MS spectrometry (positive mode), showing a mass-to-charge ratio (m/z) peak of 386.9630 Da and providing clear evidence for the formation of the complex [Pd(Aqa)(DMSO)] + H^+ with a theoretical mass of 386.9635 Da (Supp. Info., Figure S3). This result also revealed the deprotonation of the amino group upon coordination of the Pd^{II} ions, resulting in the formation of a neutral **Pd-Aqa** complex.

The **Pd-Aqa** design was conceived to promote the formation of cytosine-complementary hydrogen bonds along with a central Pd-coordination bond with the cytosine-N3 atom. This strategic design aims to facilitate the formation of a stable Pd-mediated **Cyt-Pd-Aqa** base pair, mimicking the natural Watson–Crick arrangement (Scheme 2a). Consequently, we investigated the formation of **Cyt-Pd-Aqa** complex by following the reaction between **Pd-Aqa** and Cyt. The reaction was monitored using ^1H NMR spectroscopy by

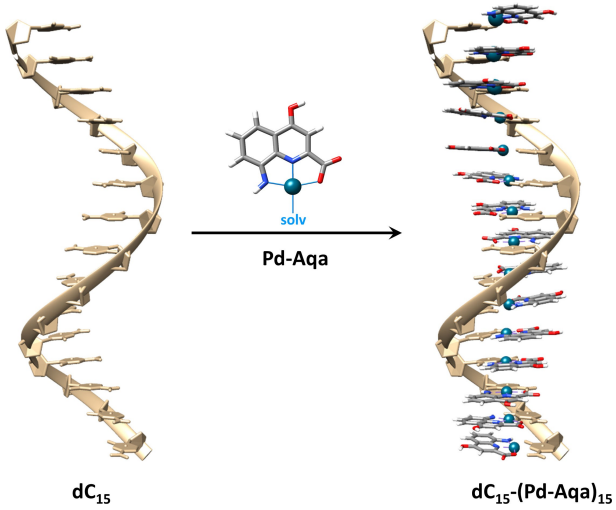

Scheme 1. Schematic representation of the self-assembly reaction between oligonucleotide **dC_{15}** and complex **Pd-Aqa**, outlining the proposed structure for the Pd-DNA hybrids.

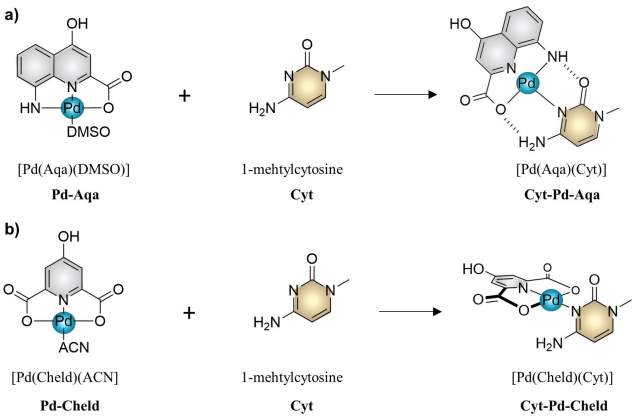

Scheme 2. Schematic representation of the formation of palladium-mediated base pairs a) [Pd(Aqa)(Cyt)] (**Cyt-Pd-Aqa**) and b) [Pd(Cheld)-(Cyt)] (**Cyt-Pd-Cheld**). (DMSO, dimethylsulfoxide; ACN, acetonitrile.)

adding controlled amounts of **Pd-Aqa** to Cyt (Supp. Info., Figure S4–S5).

The NMR (DMSO-D_6) spectra demonstrated that the Cyt signals gradually vanished while a new set emerged when **Pd-Aqa** was present. Interestingly, at equimolar quantities, the spectrum revealed the splitting of the signals, indicating the formation of two different molecular species. This was significantly evident from the observation of two different doublets for the Cyt-H5 proton at 5.97 and 5.87 ppm, and two singlets for the Aqa-H3 proton at 7.10 and 7.07 ppm. Additionally, new peaks emerged at 9.38, 8.65, 8.59, and 8.15 ppm, differing from the spectra of the free molecules. To gain further insights into these findings, we conducted NH-HSQC NMR experiment and H NMR at variable temperatures. The HSQC NMR experiment ([D_6]DMSO) facilitated the assignment of amino group hydrogen peaks, revealing that the peaks at 9.38 and 8.15 ppm can be associated with one amino group, while those at 8.65 and 8.59 ppm correspond to a different one (Supp. Info., Figure S6). The latter can be attributed to the amino group of a non-coplanar **Cyt-Pd-Aqa** arrangement formed in a smaller proportion. Similar findings were observed for the amino protons in the non-coplanar complex [Pd(Cheld)(Cyt)] (**Cyt-Pd-Cheld**), as described below. The splitting and downshift of this amino group are explained by the restricted rotation of the C-NH_2 bond upon Pd-binding at the Cyt-N3 atom. In contrast, the signals from the other amino group may be attributed to a more prevalent co-planar **Cyt-Pd-Aqa** arrangement, given their distinct separation at 9.38 and 8.15 ppm, respectively. This observation suggests the formation of a hydrogen bond with the carboxylic group of the Aqa ligand, leading to the subsequent downshift of one of the protons (at 9.38 ppm). The ^{1}H NMR spectra at variable temperatures provided additional evidence of the variable structural arrangement of the complex (Supp. Info., Figure S7). As the temperature increased, the spectrum gradually simplified, and the signals related to the amino proton groups shifted and converged into broader signals, disappearing from the downfield region at high temperatures. Remarkably, the original NMR spectra reappeared after cooling the sample back to room temperature. This solution behaviour can be explained by the varied configurations **Cyt-Pd-Aqa** can adopt. The organizational diversity arises from the rotational dynamics of the (Cyt)N3-Pd bond, a process influenced by the presence of intramolecular hydrogen bonds between the keto and amino groups of cytosine and Aqa unit. This situation prompts the **Cyt-Pd-Aqa** to adopt two conformations, including a more stable co-planar configuration stabilized by the formation of hydrogen bonds. However, the system also allows deviating from this coplanarity, leading to an equilibrium between conformations, as revealed by the NMR experiments. To date, our attempts to obtain crystals of **Cyt-Pd-Aqa** suitable for X-ray diffraction analysis have been unsuccessful. Alternatively, we employed density functional theory (DFT) calculations as an alternative approach to studying the **Cyt-Pd-Aqa** molecular arrangement. The DFT studies revealed the formation of a co-planar arrangement between the units, which was stabilized by forming intramolecular hydrogen bonds (Aqa-O···H_2N-Cyt, d_{O-H} 1.606 Å, $<_{O-H-N}$ 158° ; Aqa-NH···O-Cyt, d_{H-O} 2.108 Å, $<_{N-H-O}$ 118.3°) (Figure 1a). This co-planar configuration remained unchanged regardless of the initial dihedral angle between the units. Additionally, single-point structures resulting from incremental rotations of the cytosine ligand in 10° steps were calculated. The outcomes consistently demonstrated that the **Cyt-Pd-Aqa** complex achieves maximum stability at a dihedral angle of 0 degrees, emphasizing a clear preference for a co-planar conformation (Supp. Info. Figure S17).

Further investigations using ESI-MS spectrometry unequivocally confirm the formation of the **Cyt-Pd-Aqa** base pair, as indicated by the m/z peak found at 433.0081 Da corresponding to the $[Pd(Aqa)(Cyt)]^+$ complex (Supp. Info. Figure S8).

After preparing and studying the formation of **Cyt-Pd-Aqa** base pairs, we investigated the formation of a supramolecular Pd-DNA system. Toward this purpose, we performed a self-assembly reaction between the pentadecamer homopolymer $\mathbf{dC_{15}}$ and complex **Pd-Aqa**. The reaction was initially followed by circular dichroism titration measurements.

The CD spectrum of free $\mathbf{dC_{15}}$ exhibited a pattern with an intense positive and negative Cotton effect centred at 288 nm and 265 nm, respectively (Figure 2). Upon the controlled addition of **Pd-Aqa**, the CD profile underwent significant changes. The intensity of the original bands decreased and shifted, while a new induced band (ICD) emerged at 375 nm corresponding to the absorption of the **Cyt-Pd-Aqa** complex (Supp. Info., Figure S10), thus indicating the binding of **Pd-Aqa** to the oligonucleotide. The alteration in the CD profile stabilizes with a slight excess of more than one equivalent of **Pd-Aqa** per cytosine base, with a substantial transformation occurring for the 290 nm band when reaching an equivalence of one complex per cytosine base (Figure 2, insets). Notably, the bands maintained a similar sinusoidal shape throughout the experiment despite intensity variations. These results provide strong evidence

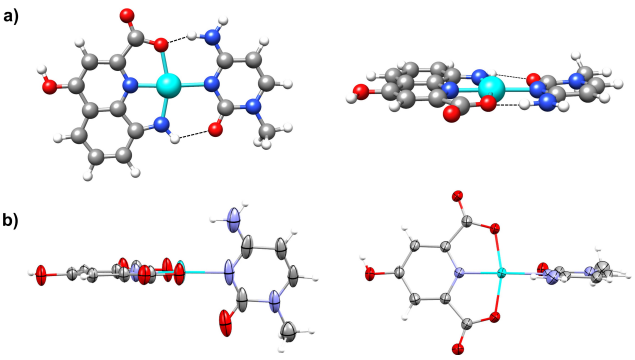

Figure 1. a) Two views for the DFT geometry-optimized structure of [Pd(Aqa)(Cyt)] (**Cyt-Pd-Aqa**). b) Two views for the X-ray structure of [Pd(Cheld)(Cyt)] (**Cyt-Pd-Cheld**), with atoms represented by ellipsoids.[18] Atom colour code: grey, carbon; white, hydrogen; blue, nitrogen; red, oxygen; cyan, palladium. Hydrogen bonds are represented by black dashed lines.

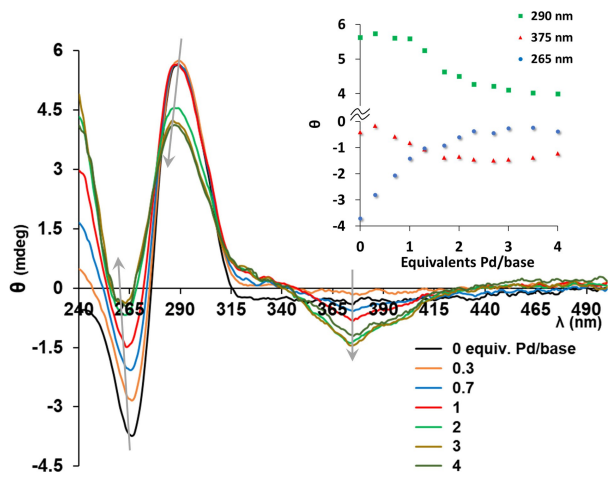

Figure 2. CD titration spectra of **dC_{15}** upon adding controlled amounts of **Pd-Aqa**. Insets: Ellipticity changes at 265, 290, and 375 nm as a function of equivalents of Pd-Aqa added. Conditions: 2 μM **dC_{15}**, 0 to 120 μM complex (in DMSO), 100 mM $NaClO_4$, 5 mM MOPS buffer pH 6.8. Note: 1 equivalent means one Pd^{II} complex per base.

for the formation of a helical **dC_{15}-(Pd-Aqa)$_{15}$** hybrid structure that closely resembles a DNA double helix. The structure is characterized by a continuous stack of **Cyt-Pd-Aqa** base pairs, reminiscent of the previously observed with **dA_{15}-(Pd-Cheld)$_{15}$** base pairs.[13] The similarity in the structural features observed in both cases suggests a consistent and reproducible self-assembly process involving cytosine-complementary **Pd-Aqa** complexes and **dC_{15}** fragment, yielding a well-defined **dC_{15}-(Pd-Aqa)$_{15}$** supramolecular structure.

ESI-MS analysis further supports the formation of the proposed structure, as evidenced by the mass spectra obtained using **dC_{15}** and a two-fold excess of the complex per base. The spectra reveal the presence of the **dC_{15}-(Pd-Aqa)$_{15}$** hybrid, alongside the occurrence of other hybrids containing a slight deficit or excess of bound complexes (Figure 3 and Supp. Info. Table S2). The presence of additional bound complexes can be attributed to the reasonable binding of palladium complexes to the cytosine amino group, as elucidated in previous studies.[19,20]

Considering all previous experimental data, we conducted density functional theory (DFT) calculations on a

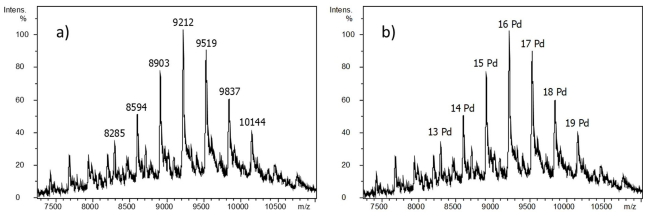

Figure 3. Deconvoluted ESI-MS spectrum recorded after incubation of **dC_{15}** (50 μM) with the **Pd-Aqa** complex (1500 μM). a) Spectrum with the experimental masses measured; b) spectrum indicating the species found, where *Pd* means one equivalent of **Pd-Aqa** per cytosine base.

dC_{12}-(Pd-Aqa)$_{12}$ supramolecular hybrid to evaluate its optimal geometry. The initial starting geometry consisted of a dodecamer oligonucleotide dC_{12} (instead of dC_{15}), representing the minimum length required to complete a helix turn while simultaneously optimizing the computational demands for the calculation. Subsequently, **Pd-Aqa** complex was bound to each base pair via Cyt-N3 atom, maintaining a co-planar arrangement between the units as described previously. Sodium cations were introduced into the system to address the ionic phosphate groups. Additionally, water molecules were strategically positioned near the donor and acceptor atoms to simulate an aqueous environment. The DFT-optimized geometry structure unveils a double-helix configuration, composed of one strand consisting of dC_{12} and the other strand comprising stacked Pd^{II} complexes, each bound explicitly to the Watson–Crick faces of the cytosine bases (Figure 4). As a result, the system forms a continuous array of Pd-mediated base pairs, with the Pd^{II} ions stacking throughout the central axis of the double helix

The resemblance of this arrangement to a natural DNA double helix is noticeable. The Pd-mediated base pairs are stacked on top of each other with a Pd···Pd distance falling within the range of 3.083–3.232 Å. The base propeller twist angles of the base pairs range from 7.42–21.3° (excluding terminal base pairs), allowing hydrogen bonds formation between the **Cyt** and **Aqa** units. The structural similarities observed in **dC_{12}-(Pd-Aqa)$_{12}$** system are comparable with our previously studied **dA_{12}-(Pd-Cheld)$_{12}$** system and underscore the consistency and reproducibility of our methodology to form supramolecular Pd-DNA-based assemblies.

Notably, the different molecular designs of our herein-reported **Pd-Aqa** complex and our previous **Pd-Cheld** complex offer an exciting opportunity for nucleobases to discriminate between the complexes, which could open the door to creating tailor-made heteroleptic metal-DNA systems. To demonstrate this concept, we investigated the relative preference of **Pd-Aqa** and **Pd-Cheld** to bind to **Cyt** and **dC_{15}**.

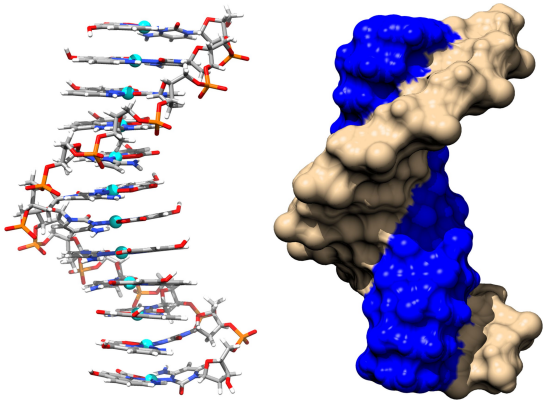

Figure 4. Left: DFT Geometry-optimized structure of **dC_{12}-(Pd-Aqa)$_{12}$** showing the organization of the **Pd-Aqa** complexes along the structure. Right: Hydrophobicity surface displaying the two different strands that form the supramolecular structure (tan; **dC_{12}**, blue; **Pd-Aqa** complexes). Sodium counterions and hydration water molecules have been omitted for clarity.

Initially, we prepared the [Pd(Cheld)(Cyt)] (**Cyt-Pd-Cheld**) complex to get insight into the structural characteristics of this base pair (Scheme 1b), using ^{1}H NMR and X-ray diffraction. The NMR spectrum analysis for the reaction between **Pd-Cheld** and Cyt showed the downshift of the cytosine's protons and the splitting of the amino signal (Supp. Info., Figure S9). These changes are consistent with the binding of **Pd-Cheld** via the Cyt-N3 atom. The non-appearance of signals at the lower field indicates the absence of intramolecular hydrogen bonds, which contrasts with the observations in complex **Cyt-Pd-Aqa** (vide supra). However, in this case, it was possible to isolate **Cyt-Pd-Cheld** in a crystalline form suitable for X-ray diffraction measurements (Supp. Info. Table S1).[18] The molecular structure reveals that the Pd^{II} ion adopts a trans-PdN2O2 square planar geometry (Scheme 1b). The **Cheld** ligand binds to Pd^{II} in a μ,κ3-N10,O2,O4-coordination mode, while the Cyt binds through its N3-atom located at the Watson–Crick face. Notably, there is a significant deviation from the coplanarity of the two ligands due to the repulsion between the keto groups, resulting in an angle of 75.63° between the r.m.s. planes of the Cyt and [Pd(Cheld)] units. This specific arrangement is responsible for the absence of intramolecular hydrogen bond formation between Cyt-amino and Cheld-keto groups. Furthermore, DFT calculations utilizing single-point structures derived from incremental rotations of the cytosine ligand consistently highlight that the most stable **Cyt-Pd-Cheld** structure deviates from coplanarity (Supp. Info. Figure S17).

Subsequently, CD titration experiments were conducted to follow the reaction between $\mathbf{dC_{15}}$ and **Pd-Cheld** and assess the formation of supramolecular $\mathbf{dC_{15}}$**-(Pd-Cheld)$_{15}$** molecules. The CD spectra showed that the addition of **Pd-Cheld** to $\mathbf{dC_{15}}$ only causes variations in the intensity of both positive and negative bands upon adding more than one equivalent of Pd-complex per base (Supp. Info., Figure S11). Moreover, these variations did not reach a stabilization point, indicating a relatively weak interaction with the oligonucleotide. It is worth noting that the complex **Cyt-Pd-Cheld** does not absorb beyond 330 nm, so the appearance of an ICD band is not expected upon the interaction (Supp. Info., Figure S10). These results suggest a weaker interaction of **Pd-Cheld** to $\mathbf{dC_{15}}$ than that observed for **Pd-Aqa** complex described previously.

Then, CD competitive binding studies were conducted to evaluate whether cytosine can discriminate between our **Pd-Aqa** and **Pd-Cheld** complexes. In the first study, controlled amounts of **Pd-Aqa** were added to a solution already containing $\mathbf{dC_{15}}$ and **Pd-Cheld** in a 1 : 1.3 ratio (Figure 5a and Supp. Info., Figure S12). Before adding **Pd-Aqa**, the initial CD spectrum exhibited the expected positive and negative bands described before, thus indicating some degree of interaction between **Pd-Cheld** and $\mathbf{dC_{15}}$. Upon adding **Pd-Aqa**, these bands underwent intensity alterations, and a new ICD band appeared at 370 nm. These changes stabilized when one equivalent of the complex was present. The resulting CD profile resembled the one previously observed for $\mathbf{dC_{15}}$**-(Pd-Aqa)$_{15}$** (Figure 2). Based on these results, it is evident that the **Pd-Aqa** complex can bind to $\mathbf{dC_{15}}$ independently of the presence of the **Pd-Cheld** fragment. In contrast, no significant changes were observed when the CD titration was reversed, i.e., when pre-formed $\mathbf{dC_{15}}$**-(Pd-Aqa)$_{15}$** was titrated with **Pd-Cheld** (Figure 5b and Supp. Info., Figure 13). This finding indicates that **Pd-Aqa** can displace **Pd-Cheld** bound to $\mathbf{dC_{15}}$ but not the other way around, suggesting a more specific and stronger binding interaction between **Pd-Aqa** and $\mathbf{dC_{15}}$. In a final experiment, an equimolar mixture of **Pd-Cheld** and **Pd-Aqa** was added to a solution containing $\mathbf{dC_{15}}$ (Figure 5c and Supp. Info., Figure S13). Once again, the resulting CD spectra profile supported the preferential formation of $\mathbf{dC_{15}}$**-(Pd-Aqa)$_{15}$**. This selectivity highlights the two complexes's distinct and

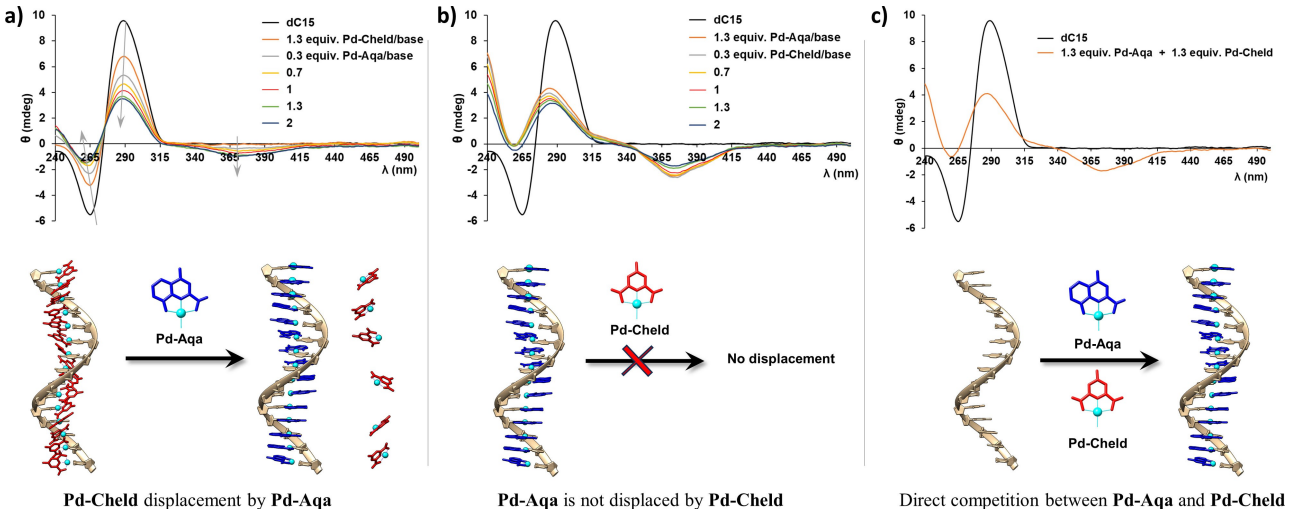

Figure 5. CD titration spectra and reaction Scheme for: a) formation of $\mathbf{dC_{15}}$**:Pd-Cheld** and subsequent addition of controlled amounts of **Pd-Aqa**, b) formation of $\mathbf{dC_{15}}$**:Pd-Aqa** and subsequent addition of controlled amounts of **Pd-Cheld**, c) $\mathbf{dC_{15}}$ upon addition of an equimolar mixture of **Pd-Cheld** and **Pd-Aqa**. Conditions: 2 μM $\mathbf{dC_{15}}$, 0–60 μM Pd-complex (in DMSO), 100 mM $NaClO_4$, 5 mM MOPS buffer pH 6.8. Note: 1 equivalent means one Pd-complex per base

non-interchangeable binding behaviours to the **dC$_{15}$** molecule.

To get more insight into the binding affinities of **Pd-Cheld** and **Pd-Aqa** towards **dC$_{15}$**, we conducted ITC experiments to measure their binding affinities and investigate the thermodynamics of these interactions (Figure 6 and Supp. Info. Figure S15). For these experiments, we used cytidine monophosphate (**CMP**) and **dC$_{15}$** and determined the thermodynamic characteristic of the palladium-mediated base pairs when they are formed isolated or along the oligonucleotide strand.

The ITC data indicated that the binding affinity between **Pd-Aqa** and **CMP**, as well as between **Pd-Cheld** and **CMP**, are very similar. The thermodynamic characteristics portrayed as binding signature plots in Figure 6b provide an understanding of these interactions (see also Supp. Info. Table S3). Enthalpic and entropic factors positively contribute to the overall binding affinity (ΔG) but, notably, the plots distinctly illustrate that the interaction with **CMP** leans predominantly towards an entropic nature. The enthalpy change (ΔH) upon binding to **Pd-Aqa** demonstrates a somewhat more favourable outcome with respect to **Pd-Cheld**.

However, since the overall binding affinities of the two compounds for CMP are very similar, the slight enthalpy distinction appears to be counteracted by an increased binding entropy (△S) associated with **Pd-Cheld**, although this difference is not significant within the error of the measurements.

The slightly higher enthalpy observed for the binding of **Pd-Aqa** to **CMP** could be attributed to the formation of intrabase hydrogen bonds (see above). Nevertheless, these hydrogen bonds make a relatively minor contribution to the overall bond enthalpy due to the necessity of breaking initial hydrogen bonds formed between the amino and keto groups and water molecules. As a result, the primary energy contribution of the binding arises from the entropy, primarily driven by the release of water accompanying the formation of the Pd-mediated base pairs.

The ITC binding curves for **CMP** were fitted with a model considering independent and equivalent binding sites (Supp. Info. Figure S15), yielding a binding stoichiometry of approximately 0.5:1 ratio (CMP:complex). These results suggest that two metal complexes can bind to **CMP**, which cannot be dismissed, given that the binding of two Pd^{II} complexes to cytidine derivatives, via the N3 atom and the amino group, has been documented.[20,21] On the other hand, the ITC analysis using oligonucleotide **dC$_{15}$** revealed an even higher binding affinity of **Pd-Aqa** compared to **Pd-Cheld** (Figure 6). Like the interaction with **CMP**, both complexes exhibit a slightly favourable binding enthalpy and a large positive entropic energy contribution upon interaction with **dC$_{15}$**. However, although the binding enthalpy is more alike, the entropic factor is now considerably higher for **Pd-Aqa**. It is well-known that cytosine-rich sequences adopt highly organized structures, even at pH 7, as observed in the CD profile for **dC$_{15}$** in the absence of complex (Figure 2).[22–24] This fact can justify the low binding enthalpies compared to higher entropy contributions. In this scenario, the relatively small loss of conformational entropy produced by **Pd-Aqa** binding could be compensated by the entropy associated with desolvation processes occurring alongside stacking events. It should be noted that, unlike the **CMP** studies, the binding to the **dC$_{15}$** strand involves the formation of stacking interactions between adjacent base pairs. The formation of **dC$_{15}$-(Pd-Aqa)$_{15}$** will exhibit more favourable stacking interactions than **dC$_{15}$-(Pd-Cheld)$_{15}$**, owing to the larger aromatic ring of the Aqa ligand, favouring the coplanarity of the rings in the **Cyt-Pd-Aqa** base pairs compared to non-coplanar **Cyt-Pd-Cheld**. These observations align with studies highlighting the importance of base-stacking interactions in DNA duplex stability.[25]

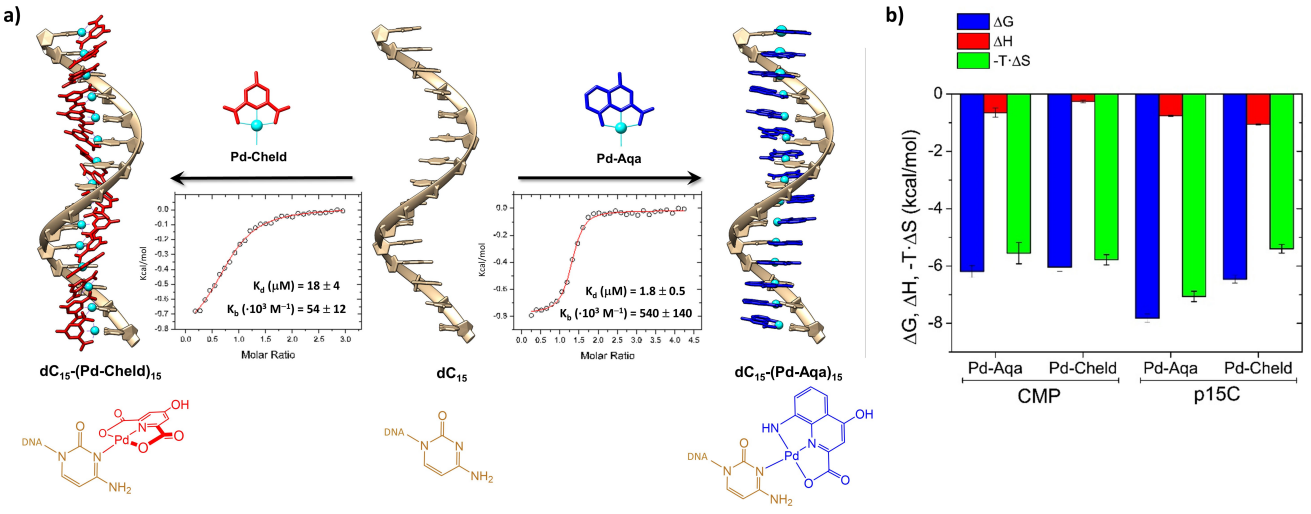

Figure 6. a) Schematic representation illustrating the binding of **dC$_{15}$** with **Pd-Cheld**, and **Pd-Cheld**, resulting in the formation of the supramolecular Pd-DNA hybrids. The Figure incorporates the titration plot versus the molar ratio of [Pd-complex]/[dC$_{15}$], obtained from the ITC profiles (Supp. Inf. Figure S14). b) The thermodynamic parameters (free energy, binding enthalpy and entropy factor) plotted for the binding of **Pd-Cheld** and **Pd-Aqa** to **CMP** and **dC$_{15}$**.

The binding stoichiometry for **dC_{15}** is now closer to $n=1$, suggesting that binding the binding of more than one Pd^{II} complex to cytidine bases is more hindered in **dC_{15}** than in free **CMP** (Supp. Info. Table S3).

The analysis of ITC data provided crucial insights into elucidating the stronger affinity of **Pd-Aqa** for **dC_{15}** compared to **Pd-Cheld**, as also observed in the CD competitive binding studies. This heightened affinity can be ascribed not only to the ability of **Pd-Aqa** to form intrabase hydrogen bonds with cytosine but also to its capacity to induce the formation of more extensive stacking interactions. These findings highlight the intricate interplay between the promotion of intramolecular hydrogen bonds and the significance of stacking interactions in the design of complementary nucleobase complexes. The latter is indispensable for stabilizing these complexes along DNA strands.

Finally, as a proof of concept for the formation of heteroleptic Pd-DNA systems, we obtained an ESI-MS spectrum illustrating the interaction between **Pd-Aqa** and **Pd-Cheld** with the oligonucleotide sequence 5′-d-(CCCACACACC)-3′ **$d(C_7A_3)$**, comprising a mixture of cytosine and adenine, specifically, seven cytosine and three adenine bases (Supp. Info. Figure S16). These preliminary results indicate that adding equal amounts of the complexes to **$d(C_7A_3)$** results in the binding of seven **Pd-Aqa** and three **Pd-Cheld** complexes, aligning with the preferential binding of the complexes to the nucleobases described herein. Nevertheless, our group is conducting ongoing research and additional experiments to deepen our understanding of this process. We are optimistic that the findings presented here will contribute to the advancement of Pd-DNA heteroleptic systems.

Conclusion

This study establishes **Pd-Aqa** as a complementary nucleobase complex capable of engaging in self-assembly reactions with polycytidine ss-DNA strands. These assemblies involve the formation of consecutive planar palladium-mediated base pairs, specifically **Cyt-Pd-Aqa** pairs, creating supramolecular Pd-DNA assemblies that closely mimic the double helix structure of natural DNA. This study's significance is underscored by the extraordinary advantage demonstrated by the purposefully designed **Pd-Aqa** complex in binding with **dC_{15}**. This complex exhibited a superior affinity for engaging with **dC_{15}**, surpassing the interaction observed with the earlier complex, **Pd-Cheld**, designed for complementary binding to adenine. These results underscore the impact of precise design in augmenting the discrimination capacity nucleobases for the binding of specific complementary complexes. Such heightened selectivity not only highlights the potential for creating heteroleptic Pd-DNA assemblies but also emphasizes the importance of strategic complex design and consideration of DNA sequence. This marks a promising avenue for future exploration in this field. From this result, our ongoing efforts are centred on the investigation of the selective binding properties of complementary nucleobase complexes to DNA sequences encompassing different nucleobases.

Supporting Information

Acknowledgements

The authors have cited additional references within the Supporting Information.[13,26–38]

Acknowledgements

Financial support from Spanish Ministerio de Ciencia e Innovación (projects PID2020-120186RB-I00 and PID2022-138479NB-I00), Junta de Andalucia (project P20_00702). We thank the "Centro de Servicios de Informática y Redes de Comunicaciones" (CSIRC) (UGRGrid), Universidad de Granada, for providing computing time on the Alhambra and Dr Ali Haidour Benamin, from Centro de Instrumentación Cientifica (UGR), for his support, assistance, and expertise in conducting NMR experiments.

Conflict of Interest

The authors declare no conflict of interest.

Data Availability Statement

The data that support the findings of this study are available from the corresponding author upon reasonable request.

Keywords: cytosine · metal-mediated base pairs · DNA · palladium · supramolecular chemistry

[1] X. Dai, Q. Li, A. Aldalbahi, L. Wang, C. Fan, X. Liu, *Nano Lett.* **2020**, *20*, 5604–5615.
[2] S. K. Vittala, D. Han, *ACS Appl Bio Mater* **2020**, *3*, 2702–2722.
[3] M. R. Jones, N. C. Seeman, C. A. Mirkin, *Science* **2015**, *347*, 1260901.
[4] D. A. Rusling, A. R. Chandrasekaran, Y. P. Ohayon, T. Brown, K. R. Fox, R. Sha, C. Mao, N. C. Seeman, *Angew. Chem. Int. Ed.* **2014**, *53*, 3979–3982.
[5] B. Jash, J. Müller, *Chem. Eur. J.* **2017**, *23*, 17166–17178.
[6] Z. Chen, C. Liu, F. Cao, J. Ren, X. Qu, *Chem. Soc. Rev.* **2018**, *47*, 4017–4072.
[7] S. Naskar, R. Guha, J. Müller, *Angew. Chem. Int. Ed.* **2020**, *59*, 1397–1406.
[8] Y. Takezawa, K. Mori, W.-E. Huang, K. Nishiyama, T. Xing, T. Nakama, M. Shionoya, *Nat. Commun.* **2023**, *14*, DOI 10.1038/s41467-023-40353-3.
[9] K. Mori, Y. Takezawa, M. Shionoya, *Chem. Sci.* **2023**, 1DYMMY.
[10] M. Balaz, S. Tannir, K. Varga, *Coord. Chem. Rev.* **2017**, *349*, 66–83.
[11] M. Surin, S. Ulrich, *ChemistryOpen* **2020**, *9*, 480–498.

[12] J. García Coll, S. Ulrich, *ChemBioChem* **2023**, e202300333.
[13] A. Pérez-Romero, A. Domínguez-Martín, S. Galli, N. Santamaría-Díaz, O. Palacios, J. A. Dobado, M. Nyman, M. A. Galindo, *Angew. Chem. Int. Ed.* **2021**, *60*, 10089–10094.
[14] O. Golubev, T. Lönnberg, H. Lönnberg, *J. Inorg. Biochem.* **2014**, *139*, 21–29.
[15] O. Golubev, T. Lönnberg, H. Lönnberg, *Helv. Chim. Acta* **2013**, *96*, 1658–1669.
[16] O. Golubev, T. Lönnberg, H. Lönnberg, *Molecules* **2014**, *19*, 16976–16986.
[17] A. Aro-Heinilä, T. Lönnberg, *Chem. Eur. J.* **2017**, *23*, 1028–1031.
[18] Deposition number 2313312 (for **Cyt-Pd-Cheld**) contains the supplementary crystallographic data for this paper. These data are provided free of charge by the joint Cambridge Crystallographic Data Centre and Fachinformationszentrum Karlsruhe Access Structures service. Data have also been deposited at the Crystallography Open Database (COD ID 3000467) and can be freely downloaded from www.crystallography.net.
[19] M. Krumm, I. Mutikainen, B. Lippert, *Inorg. Chem.* **1991**, *30*, 884–890.
[20] W.-Z. Shen, B. Lippert, *J. Inorg. Biochem.* **2008**, *102*, 1134–1140.
[21] S. Coşar, M. B. L. Janik, M. Flock, E. Freisinger, E. Farkas, B. Lippert, *Dalton Trans.* **1999**, 2329–2336.
[22] J. Kypr, I. Kejnovská, D. Renčiuk, M. Vorlíčková, *Nucleic Acids Res.* **2009**, *37*, 1713–1725.
[23] Y. Dong, Z. Yang, D. Liu, *Acc. Chem. Res.* **2014**, *47*, 1853–1860.
[24] T. Miyahara, H. Nakatsuji, H. Sugiyama, *J. Phys. Chem. A* **2013**, *117*, 42–55.
[25] A. Vologodskii, M. D. Frank-Kamenetskii, *Phys. Life Rev.* **2018**, *25*, 1–21.
[26] E. Greco, A. E. Aliev, V. G. H. Lafitte, K. Bala, D. Duncan, L. Pilon, P. Golding, H. C. Hailes, *New J. Chem.* **2010**, *34*, 2634–2642.
[27] N. P. Peet, L. E. Baugh, S. Sunder, J. E. Lewis, *J. Med. Chem.* **1985**, *28*, 298–302.
[28] APEX3 Software,V2016.1; Bruker AXS: Madison, WI, USA, **2016**.
[29] G. M. Sheldrick, *SADABS 2016/2. Program for Empirical Absorption Correction of Area Detector Data*, University Of Göttingen, Germany., **2016**.
[30] G. M. Sheldrick, *Acta Crys.* **2008**, *64*, 112–122.
[31] O. V. Dolomanov, L. J. Bourhis, R. J. Gildea, J. A. K. Howard, H. Puschmann, *J. Appl. Crys.* **2009**, *42*, 339–341.
[32] M. D. Hanwell, D. E. Curtis, D. C. Lonie, T. Vandermeersch, E. Zurek, G. R. Hutchison, *J. Cheminf.* **2012**, *4*, 17.
[33] *Avogadro: An Open-Source Molecular Builder and Visualization Tool. Version 1.2.0.* https://avogadro.cc/.
[34] E. Aprà, E. J. Bylaska, W. A. de Jong, N. Govind, K. Kowalski, T. P. Straatsma, M. Valiev, H. J. J. van Dam, Y. Alexeev, J. Anchell, V. Anisimov, F. W. Aquino, R. Atta-Fynn, J. Autschbach, N. P. Bauman, J. C. Becca, D. E. Bernholdt, K. Bhaskaran-Nair, S. Bogatko, P. Borowski, J. Boschen, J. Brabec, A. Bruner, E. Cauët, Y. Chen, G. N. Chuev, C. J. Cramer, J. Daily, M. J. O. Deegan, T. H. Dunning Jr, M. Dupuis, K. G. Dyall, G. I. Fann, S. A. Fischer, A. Fonari, H. Früchtl, L. Gagliardi, J. Garza, N. Gawande, S. Ghosh, K. Glaesemann, A. W. Götz, J. Hammond, V. Helms, E. D. Hermes, K. Hirao, S. Hirata, M. Jacquelin, L. Jensen, B. G. Johnson, H. Jónsson, R. A. Kendall, M. Klemm, R. Kobayashi, V. Konkov, S. Krishnamoorthy, M. Krishnan, Z. Lin, R. D. Lins, R. J. Littlefield, A. J. Logsdail, K. Lopata, W. Ma, A. V. Marenich, J. Martin Del Campo, D. Mejia-Rodriguez, J. E. Moore, J. M. Mullin, T. Nakajima, D. R. Nascimento, J. A. Nichols, P. J. Nichols, J. Nieplocha, A. Otero-de-la-Roza, B. Palmer, A. Panyala, T. Pirojsirikul, B. Peng, R. Peverati, J. Pittner, L. Pollack, R. M. Richard, P. Sadayappan, G. C. Schatz, W. A. Shelton, D. W. Silverstein, D. M. A. Smith, T. A. Soares, D. Song, M. Swart, H. L. Taylor, G. S. Thomas, V. Tipparaju, D. G. Truhlar, K. Tsemekhman, T. Van Voorhis, Á. Vázquez-Mayagoitia, P. Verma, O. Villa, A. Vishnu, K. D. Vogiatzis, D. Wang, J. H. Weare, M. J. Williamson, T. L. Windus, K. Woliński, A. T. Wong, Q. Wu, C. Yang, Q. Yu, M. Zacharias, Z. Zhang, Y. Zhao, R. J. Harrison, *J. Chem. Phys.* **2020**, *152*, 184102.
[35] J. P. Perdew, M. Ernzerhof, K. Burke, *J. Chem. Phys.* **1996**, *105*, 9982–9985.
[36] C. Adamo, V. Barone, *J. Chem. Phys.* **1999**, *110*, 6158–6170.
[37] S. Grimme, J. Antony, S. Ehrlich, H. Krieg, *J. Chem. Phys.* **2010**, *132*, 154104.
[38] S. Grimme, S. Ehrlich, L. Goerigk, *J. Comput. Chem.* **2011**, *32*, 1456–1465.

Manuscript received: January 4, 2024
Accepted manuscript online: January 21, 2024
Version of record online: February 5, 2024